The Astrophysical Journal, 922:131 (14pp), 2021 December 1 https://doi.org/10.3847/1538-4357/ac230e

GASP XXXV: Characteristics of the Diffuse Ionised Gas in Gas-stripped Galaxies

Neven Tomičić[1], Benedetta Vulcani[1], Bianca M. Poggianti[1], Ariel Werle[1], Ancla Müller[2], Matilde Mingozzi[3], Marco Gullieuszik[1], Anna Wolter[4], Mario Radovich[1], Alessia Moretti[1], Andrea Franchetto[1,5], Callum Bellhouse[1], and Jacopo Fritz[6]

[1] INAF-Osservatorio Astronomico di Padova, Vicolo Osservatorio 5, I-35122 Padova, Italy; neven.tomicic@inaf.it
[2] Ruhr-Universität Bochum, Faculty of Physics and Astronomy, Astronomical Institute, Universitätsstraße 150, D-44801 Bochum, Germany
[3] Space Telescope Science Institute, 3700 San Martin Drive, Baltimore, MD 21218, USA
[4] INAF-Osservatorio Astronomico di Brera, via Brera 28, I-20121 Milano, Italy
[5] Dipartimento di Fisica e Astronomia "Galileo Galilei," Università di Padova, vicolo dell'Osservatorio 3, IT-35122, Padova, Italy
[6] Instituto de Radioastronomía y Astrofísica, UNAM, Campus Morelia, A.P. 3-72, C.P. 58089, Mexico
Received 2021 April 14; revised 2021 July 16; accepted 2021 August 9; published 2021 November 25

Abstract

Diffuse ionized gas (DIG) is an important component of the interstellar medium that can provide insights into the different physical processes affecting the gas in galaxies. We utilize optical IFU observations of 71 gas-stripped and control galaxies from the Gas Stripping Phenomena in galaxies (GASP) survey, to analyze the gas properties of dense ionized gas and DIG, such as metallicity, ionization parameter log(q), and the difference between the measured log[O I]/Hα and the value predicted by star-forming models given the measured log[OIII]/Hβ (Δ log [O I]/Hα). We compare these properties at different spatial scales, among galaxies at different gas-stripping stages, and between disks and tails of the stripped galaxies. The metallicity is similar between the dense gas and DIG at a given galactocentric radius. The log(q) is lower for DIG compared to dense gas. The median values of log(q) correlate best with stellar mass and the most massive galaxies show an increase in log(q) toward their galactic centers. The DIG clearly shows higher Δ log[O I]/Hα values compared to the dense gas, with much of the spaxels having LIER/LINER-like emission. The DIG regions in the tails of highly stripped galaxies show the highest Δ log[O I]/Hα, exhibit high values of log(q), and extend to large projected distances from star-forming areas (up to 10 kpc). We conclude that the DIG in the tails is at least partly ionized by a process other than star formation, probably by mixing, shocks, and accretion of inter-cluster and interstellar medium gas.

Unified Astronomy Thesaurus concepts: Galaxy clusters (584); Galaxy groups (597); Galaxies (573); Interstellar line emission (844); Interstellar medium (847)

Supporting material: figure set

1. Introduction

Diffuse ionized gas (DIG) is a crucial but still poorly understood component of the interstellar medium (ISM) of galaxies. This gas phase is distributed across large spatial scales (up to a few kpc compared to ≈50 pc scales of star-forming associations; Levy et al. 2019), with lower gas densities ($\rho \sim 10^{-1}$ cm^{-3}) and higher temperatures ($\gtrsim 10^4$ K) than H II regions[7] (Collins & Rand 2001; Reynolds et al. 2001; Haffner et al. 2009; Barnes et al. 2014; Della Bruna et al. 2020). Other defining characteristics of DIG include lower surface brightness of the Balmer emission line Hα, higher [S II]/Hα and [N II]/Hα line ratios ([S II] λ6717,6731/H$\alpha > 0.2$) compared to the H II regions (Reynolds 1984; Reynolds & Cox 1992; Martin 1997; Madsen et al. 2006; Tomičić et al. 2017; Kreckel et al. 2016; Kumari et al. 2019; Levy et al. 2019).

There is no consensus in the literature about the main sources of ionization in DIG. The process is likely manifold, and a number of sources have been proposed. In highly star-forming galaxies, DIG can be mostly ionized by photons escaping from H II regions (Reynolds & Cox 1992; Minter & Balser 1998; Haffner et al. 2009; Relaño et al. 2012). However, the picture is more complex in early-type galaxies or in the bulges of spirals. In early-type galaxies with detected emission lines, where DIG usually comprises most of the ISM, photons from hot, low-mass evolved stars (HOLMES; Flores-Fajardo et al. 2011; Singh et al. 2013; Belfiore et al. 2017a; Zhang et al. 2017) can generally account for all of the observed *H*α emission (Cid Fernandes et al. 2011), with the rare exception of early-type galaxies undergoing rejuvenation events (Herpich et al. 2018; Werle et al. 2020), where H II regions may contribute to the ionizing field. Using data from the CALIFA survey (Calar Alto Legacy Integral Field Area), Lacerda et al. (2018) also found ionization consistent with HOLMES in spirals, especially at low galactocentric distance. Other possible sources include supernova shocks and turbulence (Slavin et al. 1993; Minter & Spangler 1997; Otte et al. 2002; Hoopes & Walterbos 2003), along with magnetic reconnection (Raymond 1992), collisional excitation from the electrons scattered from dust grains (Weingartner & Draine 2001), and cosmic rays (Barnes et al. 2014). Furthermore, some observations indicate that the emission line ratios and temperature typical of DIG could be produced by a turbulent mixing of the different hot and cold layers occuring as an aftermath of the interaction of the intra-cluster medium (ICM) and ISM (Cowie & Songaila 1977; Slavin et al. 1993; Binette et al. 2009; Fumagalli et al. 2014; Fossati et al. 2016; Consolandi et al. 2017; Campitiello et al. 2021; Müller et al. 2021).

DIG contributes with a fraction of 20% to 90% of the total Hα flux in galaxy disks, with a mean fraction around 50%–60% (Hoopes & Walterbos 2003; Oey et al. 2007; Sanders et al. 2017; Tomičić et al. 2017; Poetrodjojo et al. 2019; Della Bruna et al. 2020; Tomičić et al. 2021). This large contribution may cause star formation rates (SFRs) to be overestimated as Hα flux from DIG

[7] H II regions have temperatures of ≈10^4 K and electron densities of ≈ 100 cm^{-3} (Hummer & Storey 1987; Scaife 2013).

may be wrongly associated with star formation. There is a debate about the extent to which DIG affects measurements of gas-phase metallicity and its radial slope (Searle 1971; Vila-Costas & Edmunds 1992; Sánchez et al. 2014; Belfiore et al. 2017b; Sanders et al. 2017; Sánchez-Menguiano et al. 2018; Zhang et al. 2017; Vale Asari et al.2019; Kumari et al. 2019; Poetrodjojo et al. 2019) as some observations indicate lower metallicity (up to 1 dex) in DIG compared to nearby H II regions. DIG may also exhibit different values of line ratios and ionizing parameter log (q), further affecting observations and analysis of ISM characteristics as well as adding scatter in the distribution of galaxy properties measured from unresolved observations (Martin 1997; Flores-Fajardo et al. 2011; Dopita et al. 2014; Zhang et al. 2017; Poetrodjojo et al. 2018; Mingozzi et al. 2020). Furthermore, the detection of gas that shows different line ratios and ionization parameters located at large distances from H II regions—larger than the thickness of a typical galactic disk (≈ 1 kpc)—would indicate that sources other than star-forming (SF) regions are ionizing such gas (for example HOLMES, shocks, or mixing of different gas layers; Flores-Fajardo et al. 2011; Zhang et al. 2017; Poetrodjojo et al. 2018; Poggianti et al. 2019a). Different galactic characteristics (like mass, SFR, age, etc.) and external physical processes, such as galaxy interactions and gas stripping caused by ram pressure (Gunn et al. 1972; Toomre & Toomre 1972), may affect the ionization parameter and various line ratios (Maier et al. 2006; Nagao et al. 2006; Flores-Fajardo et al. 2011; Zhang et al. 2017; Sánchez 2020).

Recent developments in observational astrophysics, especially in the field of integral field unit (IFU) spectroscopy, have helped to probe the physics of the ISM and DIG in galaxies with better spatial and spectral resolutions (Slavin et al. 1993; Weingartner & Draine 2001; Hoopes & Walterbos 2003; Binette et al. 2009; Bundy et al. 2015; Lacerda et al. 2018; Sánchez 2020, etc.). In particular, large IFU surveys such as MaNGA (Mapping Nearby Galaxies at Apache Point Observatory; Bundy et al. 2015) and CALIFA have allowed DIG studies in statistical samples that include a variety of galaxy types.

An IFU survey that stands out due to its sample selection is the GASP project (GAs-Stripping Phenomena in galaxies with MUSE; Poggianti et al. 2017), based on Multi-Unit Spectroscopic Explorer (MUSE; Bacon et al. 2006) observations. GASP is a multi-wavelength survey that studies gas-stripping processes in 114 galaxies spanning the stellar mass range $10^9 < M_*/M_\odot < 10^{11.5}$ at redshift $0.04 < z < 0.1$ in clusters (from the WINGS and OMEGAWINGS surveys; Fasano et al. 2006; Gullieuszik et al. 2015) and the field (from the PM2GC catalog; Calvi et al. 2011). The project targets galaxies in a variety of environments (isolated; in filaments, groups, and clusters; and in junctions of the cosmic web; Poggianti et al. 2017; Vulcani et al. 2021) that are subject to different levels of ram-pressure stripping, galactic interaction, and evolution. All of these characteristics make GASP the ideal data set for studying star formation and DIG in ram-pressure-stripped tails and provide insights on how (and to what extent) DIG properties are shaped by the physical processes that drive galaxy evolution.

In Tomičić et al. (2021, hereafter GASP XXXII), we focused on measuring the fraction of Hα flux associated with DIG (hereafter $C_{\rm DIG}$) in 71 GASP galaxies. In this paper, we aim to further analyze the properties of dense gas and DIG in this galaxy sample (Section 2). First, we will analyze log(q), defined here as the ratio of the hydrogen-ionizing photon density over the local hydrogen gas density, and Δ log[O I]/Hα, defined here as the horizontal distance of the OI/Hα values from the BPT-[O I] line (Kewley et al. 2006) that separates SF and LINER/LIER regions (Section 2). We will use both spaxel-by-spaxel (Section 3.2) and integrated data (Sections 3.5 and 3.6) of the galaxies. Second, following the results of Zhang et al. (2017), we aim to test if the gas-phase metallicity differs between dense gas and DIG at a specific galactocentric radius (Section 3.4). Third, we will compare the properties of dense gas and DIG in the disk and the tails in order to understand whether ram-pressure stripping affects their properties. Furthermore, we will check if the distance from SF regions affects variation in the line ratios as a result of DIG being ionized by sources other than SF regions (Section 3.3). The discussion of the results and our conclusions are written in Sections 4 and 5, respectively.

In this paper we adopted standard cosmological constants of $H_0 = 70$ km s^{-1} Mpc^{-1}, $\Omega_M = 0.3$, $\Omega_\Lambda = 0.7$, and the initial mass function (IMF) from Chabrier (2003).

Table 1
Explanation of J-stage Numbers Used in This Paper and Number of Galaxies With J-stage Number

J Stage	Explanation	Number of Galaxies
0	non-stripped, control galaxies	30
0.5	early stage of stripping	10
1	clear gas-stripped galaxies	11
2	jellyfish galaxies	16
3	truncated galaxies	4

Note. (Defined by B.M. Poggianti et al. 2021, in preparation).

2. Data

2.1. Galaxy Sample

For this paper, as in Vulcani et al. (2018a), we consider galaxies with gas-stripping features (hereafter referred to as stripping galaxies) and compare them to undisturbed galaxies that do not show any sign of interactions or gas stripping on their Hα maps (referred to as control-sample galaxies). Galaxies that are tidally interacting with others, merging, lopsided, or cosmic-web-enhanced are not included in this paper (Vulcani et al. 2017, 2018b, 2018c, 2019a, 2020, 2021).

For each galaxy, B. M. Poggianti et al. (2021, in preparation) have designated a specific number indicating a stage of stripping referred to here as J-stage number (Table 1). The J-stage numbers classify non-stripped galaxies as 0, galaxies in early stages of stripping as 0.5, clear gas-stripped galaxies and jellyfishes as 1 and 2, respectively, and galaxies with a truncated Hα disk as 3. Truncated galaxies are galaxies where the gas disk was mostly stripped, except in the galactic center (Koopmann & Kenney 2004; Fritz et al. 2017). We will use this classification system in this paper to compare galaxies at different stripping phases.

Both stripping and control samples are drawn from Vulcani et al. (2018a) with some modifications. The stripping sample is composed of 41 galaxies. With respect to Vulcani et al. (2018a), we exclude JO149 and JO95 since we are not able to measure their effective galactocentric radii and orientation (Franchetto et al. 2020). Furthermore, we add JO93 (a member of the control sample in Vulcani et al. 2018a) because its Hα map indicates an initial phase of stripping.

The control sample includes 30 galaxies, 16 of which are cluster members and 14 are field galaxies. With respect to

Vulcani et al. (2018a), we exclude P19482, as Vulcani et al. (2019b) showed that the galaxy is not undisturbed but undergoing cosmic-web enhancement. The control-sample galaxies by definition have no tails.

2.2. Observations, Line-maps, and Galaxy Orientation

The galaxies were observed by MUSE, an IFU at ESO-VLT (the Very Large Telescope of the European Southern Observatory), covering the optical range of 4800–9300 Å. The data analysis of the observed cubes follows established procedures described in Poggianti et al. (2017). Briefly, the observed spectrum in each spaxel of the cube was corrected for the effect of foreground dust extinction of the Milky Way, with corresponding E_{B-V} values for each galaxy in the line of sight (LOS) on-sky measured by Schlegel et al. (1998), considering the recalibration introduced by Schlafly & Finkbeiner (2011) and assuming the extinction curve of Cardelli et al. (1989) with $R_V = 3.1$. To account for seeing effects, the data were smoothed and convolved in the spatial dimension using a 5×5 pixel kernel, which corresponds to 1″, or 0.7–1.3 kpc, depending on the galaxy's redshift.

The convolved cubes were analyzed with the spectro-photometric code SINOPSIS (Fritz et al. 2017) to fit the stellar component of the spectra, and then with KUBEVIZ (Fossati et al. 2016) to fit the gas emission lines in the stellar-continuum subtracted spectra. The emission lines used in this work are: Hβ, [O III]λ5007, [O I]λ6300 (referred hereafter as [O I]), Hα, [N II]λ6584, and [S II]λ6713,6731 (referred hereafter as [S II]).

Maps of Hα surface brightness corrected for attenuation, labeled as $\Sigma H\alpha$, *corr*, were calculated assuming the intrinsic Balmer line ratio Hα/H$\beta = 2.86$, ionized gas temperature of $T \approx 10^4$ K and case B recombination (Hummer & Storey 1987; Osterbrock & Martel 1992). We applied a cut in signal-to-noise S/N $\geqslant 4$ for all emission lines in our analysis and for our results.

The boundaries of stellar disks were estimated using an isophote in the continuum maps that is 1σ above the average sky background noise and the center of the galaxies is designated to be the centroid of the brightest central region in the continuum map (Gullieuszik et al. 2020). We define the spaxels (with the ionized gas emission) outside the stellar disks as part of the galactic tails. The disk inclination with respect to the line of sight and the disk diameter were estimated by Franchetto et al. (2020) from the *I*-band images obtained by convolving the MUSE data cube spectra.

It is important to note that a clear separation between DIG and H II regions requires a resolution that is not achieved by our observations. Thus we can only probe regions where H II complexes and DIG are mixed together in the line of sight and measure the DIG emission fraction instead. Therefore, in this paper we use the terms "dense gas" and DIG, not H II regions and DIG.

2.3. Metallicity, Ionization Parameter, and $\Delta \log[O\,I]/H\alpha$

Two of the main quantities of interest in our analysis are the gas-phase metallicity and ionization parameter. These quantities were derived from the emission line ratios, [O III]λ5007/[S II] versus [N II]λ6583/[S II], using the PYQZ code (v0.8.2 version, Dopita et al. 2013; Vogt et al. 2015). We assume solar metallicity to be $12 + \log(O/H) = 8.69$. Details on how we estimate the gas-phase metallicity and log(q) for the GASP sample are described by Franchetto et al. (2020). log(q) is defined as the logarithm of the ratio of the hydrogen-ionizing photon density (in cm^{-3}) over the local hydrogen gas density (in cm^{-3}) multiplied by the speed of light (Kewley et al. 2006; Nagao et al. 2006; Kewley et al. 2019). Since it measures the ratio of ionization intensity and gas density, it may be used as an indication for the ratio of radiation and gas pressures (Yeh & Matzner 2012). We note that PYQZ uses photoionization models of line ratios that assume ionization with photons from SF regions.

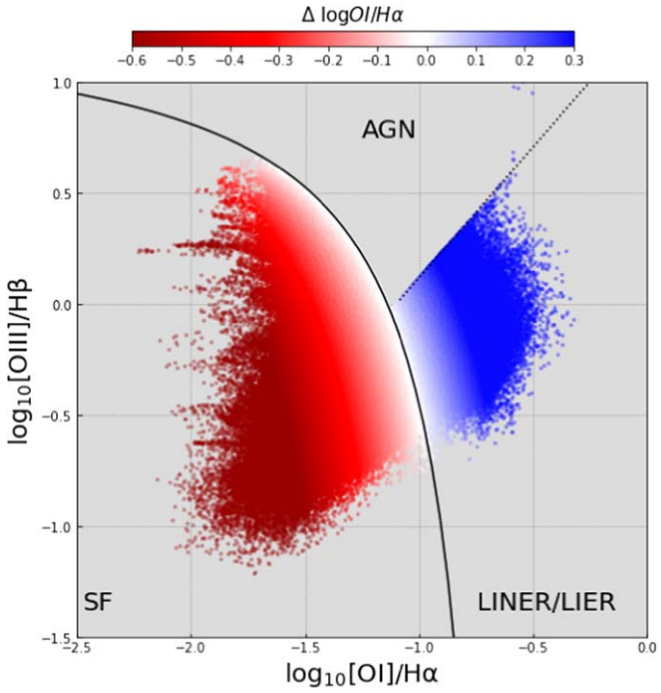

Figure 1. BPT-[OI] diagram of the spaxels of all galaxies, color-coded by Δ log[O I]/Hα values. The Δ log[O I]/Hα value is defined here as the horizontal distance of the O I/Hα values from the BPT-[O I] line (thick black line; Kewley et al. 2006) that separates SF and LINER/LIER regions. The dashed black line separates AGN regions from LINER/LIER regions (Kewley et al. 2006).

The Baldwin, Phillips, and Terlevich diagnostic diagrams (BPT; Baldwin et al. 1981; Kewley et al. 2006) of emission line ratios are used to infer the dominating ionization mechanism, such as SFs, AGNs, or LINERs[8]/LIERs[9]. In this work, we only use the BPT diagram based on the [O I]λ6300 line (hereafter BPT-[O I], shown in Figure 1), and we removed spaxels dominated by AGN ionization. The [O I]/Hα line ratio is sensitive to the hardness of the ionizing radiation field (Kewley et al. 2006) and LINER/LIER-like spaxels may potentially indicate that the origin of ionization across the galaxy disks and tails can be other than SF regions.

To quantify the difference in ionization source and variation in gas emission among the galaxies, for each spaxel we measure the difference between the measured log[O I]/Hα and the corresponding value on the BPT-[O I] line that separates the SF and LINER/LIER region,[10] at the measured log[OIII]/Hβ. This value is called Δ log[O I]/Hα and is shown in Figure 1. Negative Δ log[O I]/Hα values represent regions defined as SF, while positive values represent LINER/LIER-like regions. We note that negative Δ log[O I]/Hα does not necessarily

[8] Low-ionization nuclear-emission regions (Heckman & Balick 1980).
[9] Low-ionization emission regions (Belfiore et al. 2016).
[10] This line was computed as an upper limit of the theoretical pure stellar photoionization models in the starburst case (Kewley et al. 2001, 2006).

mean that the ionization is coming only from SF regions, but that these account for the largest fraction. Similarly, LINER/LIER-like regions do not exclude a possibility of partial ionization by star formation. The individual BPT diagrams of spatially resolved data for 16 GASP galaxies were shown by Poggianti et al. (2019b).

2.4. Fraction of the Diffuse Ionized Gas

In GASP XXXII, we estimated the fraction of Hα emission coming from DIG for all 71 galaxies studied in this work. The initial assumption was that the DIG exhibits lower $H\alpha_{\rm corr}$ flux surface density (Σ Hα) and higher [S II]/Hα line ratio than the dense gas (Blanc et al. 2009; Kaplan et al. 2016). We account for the radial gas-phase metallicity distribution across the galaxy, where we divided the [SII]/Hα ratio by the gas metallicity value at each given radial bin. Then we fitted the spaxel-by-spaxel anti-correlation between the [S II]/Hα ratio and the extinction-corrected ΣH$\alpha_{\rm corr}$ for each individual galaxy. For this fitting, we designated the spaxels with the highest [SII]/Hα ratio and lowest ΣH$\alpha_{\rm corr}$ to have $C_{\rm DIG} = 1$, while the data with the highest ΣH$\alpha_{\rm corr}$ were assumed to have low $C_{\rm DIG}$ fraction. We then derived the relation between the DIG fraction and ΣH$\alpha_{\rm corr}$ and created maps of $C_{\rm DIG}$ from the ΣH$\alpha_{\rm corr}$ maps. Further details of the method can be found in GASP XXXII.

In principle, considering metallicity as a parameter in our method to estimate $C_{\rm DIG}$ could introduce a bias in our analysis of $C_{\rm DIG}$ versus metallicity. However, at a given radius, the metallicity correction affects the [S II]/Hα of dense-gas and DIG spaxels equally, thus not changing the slope of the spaxel-by-spaxel anti-correlation in the diagrams. Furthermore, our method uses both [S II]/Hα and Hα, thus mitigating strong effects of metallicity on $C_{\rm DIG}$ and lowering the scatter of the data. Thus, the $C_{\rm DIG}$ values in spaxels at similar radii are not significantly affected by variations in metallicity.

In what follows, to clearly contrast regions whose emission is generated by different mechanisms, we will consider dense-gas-dominated spaxels those with $C_{\rm DIG} \leqslant 0.3$, DIG-dominated spaxels those with $C_{\rm DIG} > 0.7$, and disregard the spaxels with intermediate values.

3. Results

In this section we will investigate galaxy metallicity, log(q), and Δ log[O I]/Hα across our galaxy sample. We will first consider spatially resolved (i.e., spaxel-by-spaxel) scales, and then values at larger spatial scales (radial trends and integrated values). Furthermore, we will compare (i) regions dominated by dense-gas emission with those dominated by DIG emission, (ii) disks and tails of galaxies, (iii) different stages of stripping (J stage) in the stripping sample. Lastly, we will investigate trends of log(q) and Δ log[O I]/Hα with integrated values such as stellar mass, SFR, and metallicity measured at the effective radius. Only spaxels ionized by SF processes (according to BPT-[O I]) are considered when the metallicity and log(q) are analyzed and displayed (spaxel-by-spaxel or integrated values).

3.1. Maps of Galaxies

We present the maps of $C_{\rm DIG}$, Δ log[O I]/Hα, and log(q) values for control (A3376_B_0261) and stripped galaxies (JO175, JO85) in Figure 2, and all other galaxies in the figure set. We indicate the control and stripped samples with thin and thick line edges of panels, respectively. We will further quantify the trends of Δ log[O I]/Hα and log(q) as a function of galactocentric radius in Section 3.4.

The maps of $C_{\rm DIG}$ (left panels of Figure 2 and the figures in the Appendix) reveal some interesting trends: in most cases, the dense gas is confined to the galaxy's core and spiral arms, and DIG emission is preferentially found between the arms, in the galaxy's outskirts, and in tails of stripped galaxies. The maps are lacking Δ log[O I]/Hα values (middle panels) in many spaxels compared to the $C_{\rm DIG}$ map due to a low S/N of [O I] emission line.

Comparing the maps of $C_{\rm DIG}$ and those of Δ log[O I]/Hα and log(q), we recover a tendency for the dense-gas-emission-dominated areas to have higher ionization parameters and lower Δ log[O I]/Hα than the DIG-dominated areas. Moving from galaxy cores to the outskirts and tails, the incidence of LINER/LIER-like spaxels (higher Δ log[O I]/Hα values) increases and log(q) decreases.

3.2. Spaxel-by-spaxel Comparison

Figure 3 compares the spatially resolved Δ log[O I]/Hα for dense-gas-dominated spaxels (blue, filled histograms) and DIG-dominated spaxels (red, hatched histogram), for different regions (disks and tails) of the control and stripped galaxies. We remind readers that control sample galaxies have no tails by definition. The median values of the corresponding distributions are represented by the blue and red vertical lines for the dense-gas and DIG-dominated spaxels, respectively.

While dense gas in disks of the control galaxies shows median Δ log[O I]/H$\alpha \approx -0.5$, disks and tails of the stripped galaxies have median Δ log[O I]/Hα of ≈ -0.4 and ≈ -0.3 respectively. In general, the DIG-dominated spaxels have ≈ 0.4 dex higher median Δ log[O I]/Hα than dense-gas areas. The DIG spaxels in the disks show more LINER-like spaxels (approximately half of the spaxels), while the stripped tails show the majority (83%) of spaxels with positive Δ log[O I]/Hα.

3.3. Δ log[O I]/Hα and Distance from SF Regions

In star-forming galaxies, DIG can reach scale heights of $1-2$ kpc (Reynolds 1984; Haffner et al. 2009; Bocchio et al. 2016; Tomičić et al. 2017), which is larger than the thickness of stellar disks (up to a few hundreds of pc), favoring the hypothesis that DIG could require ionization by sources other than star formation (i.e., older stellar populations or mixing of ISM and ICM). Detecting DIG at large distances from SF regions would validate that hypothesis.

In this section we consider only the DIG-dominated spaxels and characterize their projected distance[11] from SF regions (designated by the BPT-[O I] diagram). For each individual non-SF spaxel, we measure the mean distance from the closest 10 SF spaxels. Figure 4 presents Δ log[O I]/Hα values of spaxels in all galaxies as a function of the projected distance from the SF spaxels.

As in Figure 3, we show data for different types of galaxies (control versus stripped) and their different parts (disks versus tails). In general, we notice a positive trend between Δ log [O I]/Hα and distance. In the stripped tails and in some parts of the stripped galaxies' disks, there are regions that span large distances from the SF spaxels (>2 kpc and up to 10 kpc), and which have a mean Δ log[O I]/Hα value of ≈ 0.4. These

[11] Due to the uncertainty of projections of lengths, this measured distance is a lower limit.

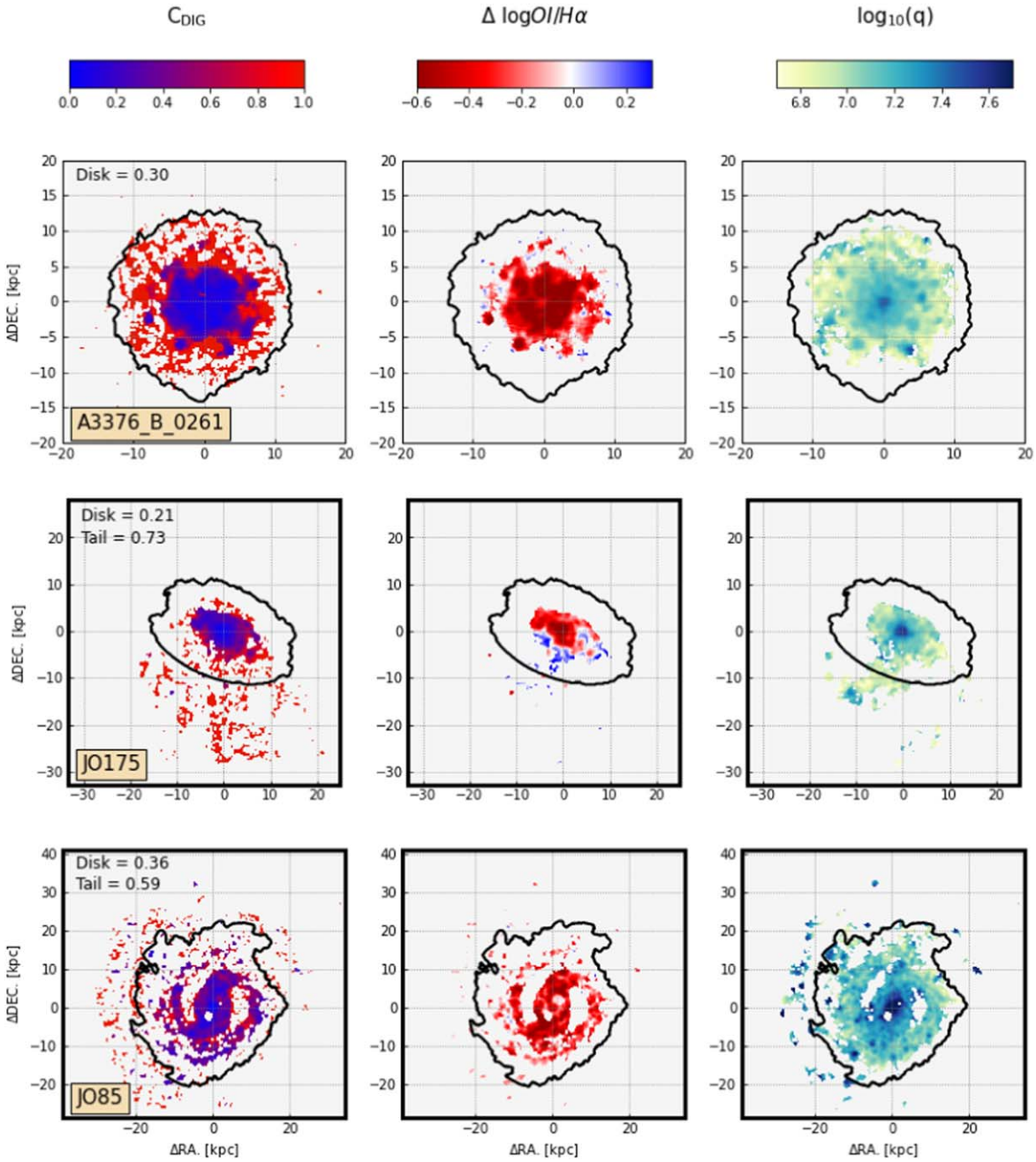

Figure 2. Galaxies presented here are A3376_B_0261, JO175, and JO85. The panels showing control-sample and stripped galaxies have thin and thick edges, respectively. The ticks on the axes are centered in relation to the galactic center. We indicate the galactic disk with the thick, black contour (see text for the definition). Left column: Maps of the diffuse ionized gas fraction (C_{DIG}), from Tomičić et al. (2021). Dense-gas-dominated spaxels are blue, while DIG-dominated spaxels are red. The integrated C_{DIG} values for the disks and tails are labeled in the upper left corner. Central column: Maps of Δ log[O I]/Hα, which measures distances of O I/Hα values from the BPT-[O I] line that separates SF and LINER/LIER regions. Right column: Ionization parameter log(q) maps. The complete figure set (18 images) is available in the online journal. It contains the same maps for all the other galaxies in the sample.

(The complete figure set (18 images) is available.)

spaxels, which exhibit high Δ log[O I]/H$\alpha \approx 0.4$ and are distant from the SF regions, correspond to highly stripped galaxies (JO93, JW100, JO204, JO194, JO147, JO85, JO60, JO27), of which the edge-on JW100 with its long tail contributes the most (approximately half of those spaxels).

From these results, we conclude that DIG in stripped galaxies extends to very large distances from SF regions, which would make its ionization by SF regions alone less probable.

3.4. Comparing DIG and Dense-gas Properties at Different Galactocentric Radii

Next, we test if regions dominated by DIG and dense-gas emission in disks of both control and stripped galaxies are also characterized by different values of gas-phase metallicity, log (q), and Δ log[O I]/Hα, at each given galactocentric distance.

We divided the spaxels into annuli of different deprojected galactocentric radii (normalized by the effective radius of the

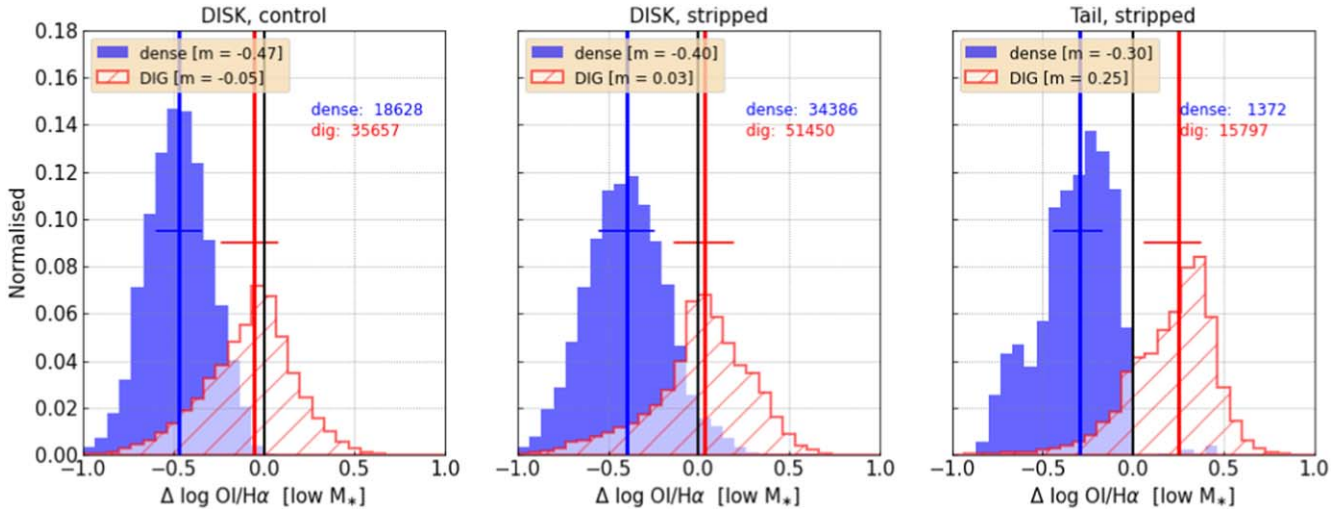

Figure 3. Histograms of spaxel-by-spaxel comparison of $\Delta \log[\mathrm{O\,I}]/\mathrm{H}\alpha$ values for dense gas (filled, blue) and DIG (hatched, red) across the galaxies. There are 244,479 spaxels in total. The data are separated according to location from where they were sampled: disks of the control sample (left), disks (middle), and tails (right) of the stripped galaxies. The corresponding median values and the range between first and third percentile are indicated by vertical and horizontal blue (dense gas) and red (DIG) lines, and they are labeled in the legend of the panels. The numbers of spaxels in corresponding distributions are labeled in the upper right corner of the panels.

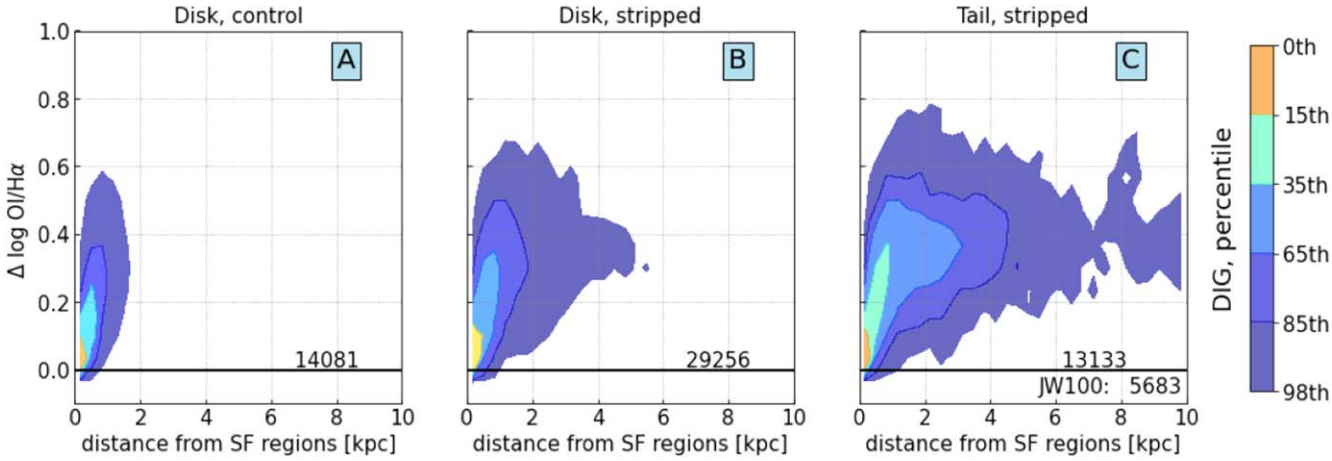

Figure 4. Spaxel-by-spaxel comparison of $\Delta \log[\mathrm{O\,I}]/\mathrm{H}\alpha$ (y-axis) and the distance from the SF regions (x-axis) for DIG-dominated spaxels in the galaxies. The contours represent the 15th, 35th, 65th, 85th, and 98th percentiles of their spaxel distributions. The numbers of spaxels in corresponding distributions are labeled in the bottom right corner of the panels. We separately included the number for JW100.

disk; Franchetto et al. 2020). In each radial annulus, we measured the median of all quantities as well as differences between median values of DIG and dense-gas-dominated spaxels. We present in Figure 5 the absolute values (left panels) and the differences between median values of dense gas and DIG (right panels) as a function of radial annuli. The figure shows each galaxy separately as a data point, color-coded by its stellar mass (blue for $\log M_* < 10.3$ and orange for $\log M_* \geqslant 10.3$).

For the gas-phase metallicity (upper panels), the absolute values decrease with radius, as expected from the fact that metallicity gradients are negative for the great majority of galaxies (Mingozzi et al. 2020, A. Franchetto et al. submitted). The low-mass galaxies have lower metallicities, following the known mass–metallicity relation (Franchetto et al. 2020). A small difference (< 0.05 dex) between the DIG- and dense-gas-dominated spaxels is detected, but no variation of this difference with galactocentric radius is found. The scatter of the data (≈ 0.5 dex) and the uncertainty of individual data points (≈ 0.1 dex) are larger than the difference in metallicities between dense gas and DIG.

The ionization parameter (middle panels) does not show a clear trend with radius for low-mass galaxies but shows a clear decrease with radius for the high-mass galaxies. The difference in $\log(q)$ between DIG and dense-gas areas shows a negative offset, with DIG data having ≈ 0.1 dex lower values. Furthermore, the $\log(q)$ offset between DIG and dense gas increases with galactocentric radius.

Mean absolute values of $\Delta \log[\mathrm{O\,I}]/\mathrm{H}\alpha$ (bottom panels) increase with radius for galaxies of all masses by ≈ 0.2 dex. At a given radius, the high-mass galaxies tend to have slightly lower values compared to the low-mass galaxies. The offset in $\Delta \log[\mathrm{O\,I}]/\mathrm{H}\alpha$ indicates that DIG-dominated regions have 0.2–0.3 dex higher $\Delta \log[\mathrm{O\,I}]/\mathrm{H}\alpha$ values compared to dense-gas-dominated regions and the mean value of this difference increases with radius.

These results indicate that metallicity is not affected by the DIG fraction. The median $\log(q)$ of total gas increases in the centers of high-mass galaxies, with DIG fraction playing a small role in $\log(q)$. The median $\Delta \log[\mathrm{O\,I}]/\mathrm{H}\alpha$ of total gas is increasing toward the edges of all galaxies, with the DIG fraction potentially playing an important role.

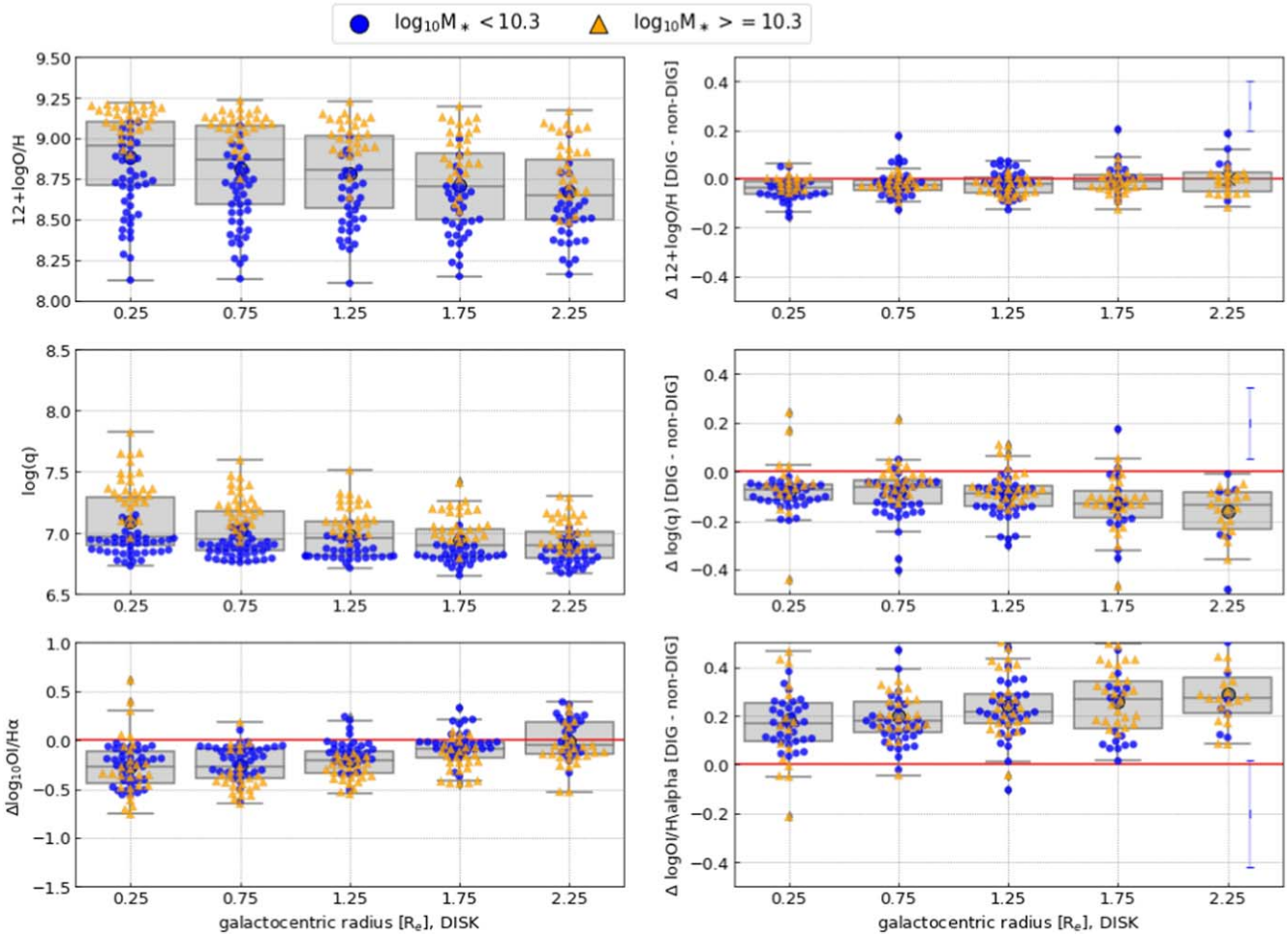

Figure 5. Median values of quantities of spaxels in the disk of each galaxy, shown as absolute values in the left panels, and as difference between DIG ($C_{\rm DIG} > 0.7$) and dense-gas- ($C_{\rm DIG} < 0.3$) dominated spaxels in the right panels. Quantities presented here are: gas-phase metallicity (upper panels), log(q) (middle panels), and Δ log[O I]/Hα values (bottom panels). The values are plotted as a function of the galactocentric radius (normalized by the effective radius R_e). Each galaxy is represented by a data point, while the quartiles and extent of all data are plotted with gray boxes and vertical lines. We color-code galaxies by their stellar-disk mass, log $M_* < 10.3$ in blue circles and log $M_* \geqslant 10.3$ in orange triangles. The mean uncertainty is plotted as the blue error bar on the right.

3.5. Galaxy Integrated Values

We investigate in Figure 6 different physical properties such as the integrated fraction of DIG emission[12] ($C_{\rm DIG,int}$, GASP XXXII) as a function of J stage (left panel), median log(q) (middle panel), and Δ log[O I]/Hα (right panel). We estimated the $C_{\rm DIG,int}$ within the disks and tails of all galaxies (control-sample and stripped galaxies). In the case of median log(q), we use the median value of only the spaxels designated as SF on the BPT-[O I] diagram.

As seen in GASP XXXII, the disks of stripped and control-sample galaxies cover a similar range in $C_{\rm DIG,int}$ (from 0.1 to 0.9), with a median value[13] $C_{\rm DIG,int} = 0.44^{0.52}_{0.33}$ for the entire sample. The tails of stripped galaxies have higher DIG fractions (median $C_{\rm DIG,int} = 0.83^{0.99}_{0.69}$) than the disks.

There is generally no systematic variation of the $C_{\rm DIG,int}$ of disks with J stage. Truncated disks ($J = 3$) show a low DIG fraction (≈ 0.2), probably due to a large fraction of gas being stripped away from the disk, and preservation of only the dense-gas, star-forming regions in their centers.

Focusing on the ionization parameter, we find that control galaxies have lower median values (log(q) $= 6.93^{7.0}_{6.88}$) compared to the stripped galaxies (median log(q) $= 7.03^{7.17}_{6.94}$). The disks and tails of the stripped sample also show the same median values. We note that the control sample spans a narrower range of log(q) than the disks and tails of stripped galaxies.

The gas in disks of control and stripped sample galaxies has mostly negative Δ log[O I]/Hα values (median $-0.22^{-0.12}_{-0.31}$ and $-0.09^{0.02}_{-0.2}$, respectively). The tails have higher values in Δ log [O I]/Hα than the disks with more than half of them having positive values (median Δ log$_{10}$ [O I]/H$\alpha = 0.0^{0.12}_{-0.06}$).

We also notice a weak correlation between Δ log[O I]/Hα and $C_{\rm DIG,int}$ across stripped galaxies (Pearson coefficient $\rho = 0.33 \pm 0.00$), while the control galaxies show a slight anti-correlation ($\rho = -0.24 \pm 0.2$). This effect is mostly due to the tails of high $C_{\rm DIG,int}$, which have slightly higher Δ log [O I]/Hα.

These results show that the gas-stripping process, in general, slightly increases the log(q) range and systematically increases the values of Δ log[O I]/Hα, especially in the tails.

[12] The integrated fraction here is defined as the sum of the Hα luminosity from DIG-dominated spaxels over the total Hα luminosity of galaxy.
[13] We show median values and first and third quartiles in diagrams above and on the right of the panels.

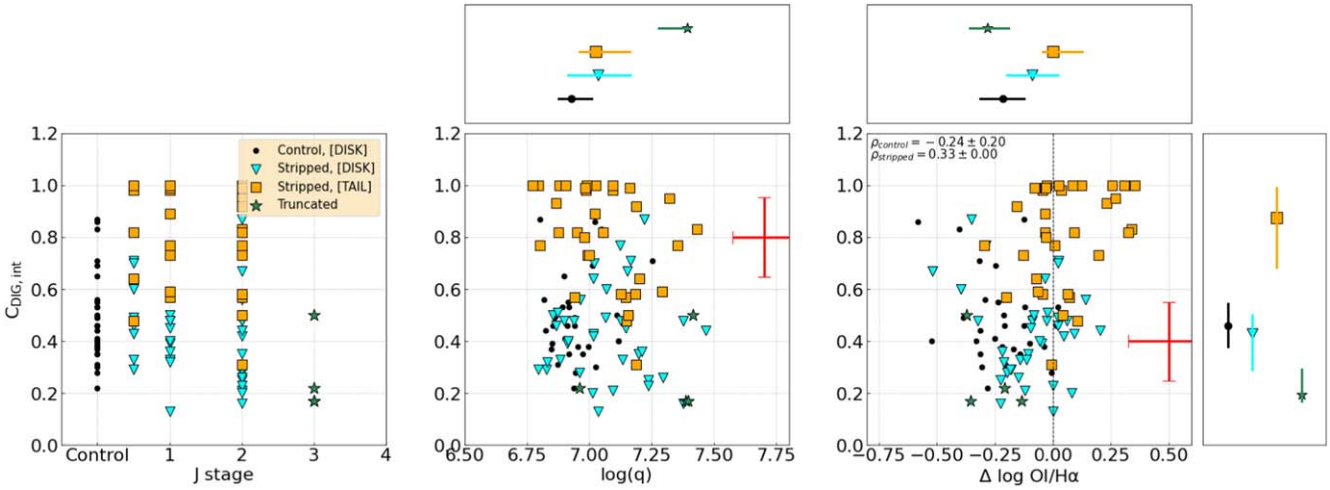

Figure 6. Diagrams of the integrated fraction of DIG emission ($C_{\rm DIG,int}$) as a function of J stage (left panel), median galactic values of $\log_{10} q$ (middle panel), and [O I] excess (right panel). We show control-sample disks (black dots), disks (cyan triangles), and tails (yellow squares) of the stripped galaxies and truncated disks (green stars). The mean uncertainty of all values is shown in the right corners of panels and Pearson coefficients in the upper left corner of the right panel. Above and on the right, we show median values and the first and third quartile of the data samples in diagrams with their corresponding symbols.

3.6. How Do log(q) and Δ log[O I]/Hα Vary with Galaxy Properties?

To investigate if log(q) and $\Delta \log[\mathrm{O\,I}]/\mathrm{H}\alpha$ vary with integrated galactic properties, we compare galaxy global values (medians of spaxels) of log(q) and $\Delta \log[\mathrm{O\,I}]/\mathrm{H}\alpha$ as a function of stellar mass, SFR, specific SFR (sSFR = SFR/$M_\star$), and other overall galaxy properties. The integrated values of log(q) and $\Delta \log[\mathrm{O\,I}]/\mathrm{H}\alpha$ as a function of stellar mass are presented in Figures 7 and 8, respectively. The comparison with other properties (SFR and sSFR of disks, gas-phase metallicity, ratio of area of tails and disks) is shown in the Appendix.

We separate panels and compare the median values of data as follows: (1) disks of control and stripped galaxy samples (panels A and C), (2) disks and tails of the stripped galaxies (panels B and D), and (3) dense-gas-dominated (panels A and B) and DIG-dominated (C and D) areas in the galaxies. We show the difference between DIG and dense-gas data in panel E, and the difference between disks and tails of the stripped galaxies in panel F. From these comparisons, we observe a few major results and trends, as follows.

The low-mass galaxies ($\log_{10} M_* \leqslant 10.3\ M_\odot$) are characterized by a rather constant value of log(q), while log(q) for the high-mass galaxies ($\log_{10} M_* > 10.3\ M_\odot$) strongly correlate with stellar mass. DIG in disks and tails has $0.1 - 0.2$ dex lower log (q) compared to the dense gas in the same environments. There is no clear difference in the evaluated gas properties in disks of control and stripped galaxies (panel E) and between the tails and disks of the stripped sample (panel F). The large scatter in the measured properties prevents a conclusive analysis of trends with stellar mass in panels E and F.

Considering $\Delta \log[\mathrm{O\,I}]/\mathrm{H}\alpha$ of the dense gas, we observe a weak anti-correlation with stellar mass (Figure 8). Furthermore, this anti-correlation is stronger for low-mass galaxies than for high-mass ones. DIG areas show higher $\Delta \log[\mathrm{O\,I}]/\mathrm{H}\alpha$ values (≈ 0.4 dex) compared to dense gas (as clearly seen in panel E), with the tails having larger offsets (by ≈ 0.1 dex) than the disks. We highlight the fact that all dense-gas data have $\Delta \log[\mathrm{O\,I}]/\mathrm{H}\alpha$ values below 0, while most of the DIG show positive values. We also notice in panel D that galaxies of higher J-stage number have higher $\Delta \log[\mathrm{O\,I}]/\mathrm{H}\alpha$ values for DIG-designated spaxels in the tails (magenta square symbols) compared to the rest of the data in other panels.

Regarding other galactic values (presented in the Appendix), log (q) correlates with SFR and gas-phase metallicity. We explain this as a signature of well-known correlations between the stellar mass, metallicity, and SFR. The dense gas shows a somewhat strong anti-correlation between $\Delta \log[\mathrm{O\,I}]/\mathrm{H}\alpha$ and metallicity and DIG exhibits a weak correlation between $\Delta \log[\mathrm{O\,I}]/\mathrm{H}\alpha$ and the spaxel fraction of tails versus disks. The former relation is most likely an effect of metallicity on the increase in $[\mathrm{O\,I}]/\mathrm{H}\alpha$ ratio.

To conclude, these results indicate that the stellar mass is driving the increase in median log(q) across the galaxies more than the fraction of DIG. Moreover, DIG clearly shows high $\Delta \log[\mathrm{O\,I}]/\mathrm{H}\alpha$ values compared to the dense gas, especially in the case of the stripped tails.

4. Summary of Results and Discussion

4.1. Variation with Gas-phase Metallicity

In the previous section we showed that gas-phase metallicity at a given galactocentric radius and at kpc spatial resolution does not vary with different DIG fractions in the disks of all galaxies (Figure 5). This would indicate two major conclusions about the distribution of the metallicity within the disks. First, DIG emission should not hinder the measurement of metallicity at a given radius in galaxies. Second, there is no difference in the metallicity radial gradient between areas dominated by dense gas or DIG.

Similar to our conclusions, Kumari et al. (2019) did not find significant differences in metallicities between spatially close-by HII-DIG/LIER pairs, which are expected to be chemically homogeneous. However, their results may be affected by a non-SF source of ionization changing line ratios used for metallicity diagnostics.

On the other hand, Poetrodjojo et al. (2019) found tentative results for different metallicity gradients in DIG- and H II-dominated spaxels of the M83 galaxy. Analyzing IFU data from MaNGA, Zhang et al. (2017) also showed that DIG can significantly bias the measurement of gas metallicity and metallicity gradients derived using strong emission lines. However, Zhang et al. (2017) used an incomplete method to separate dense gas from DIG, using only Σ Hα information. Lacerda et al. (2018) note that

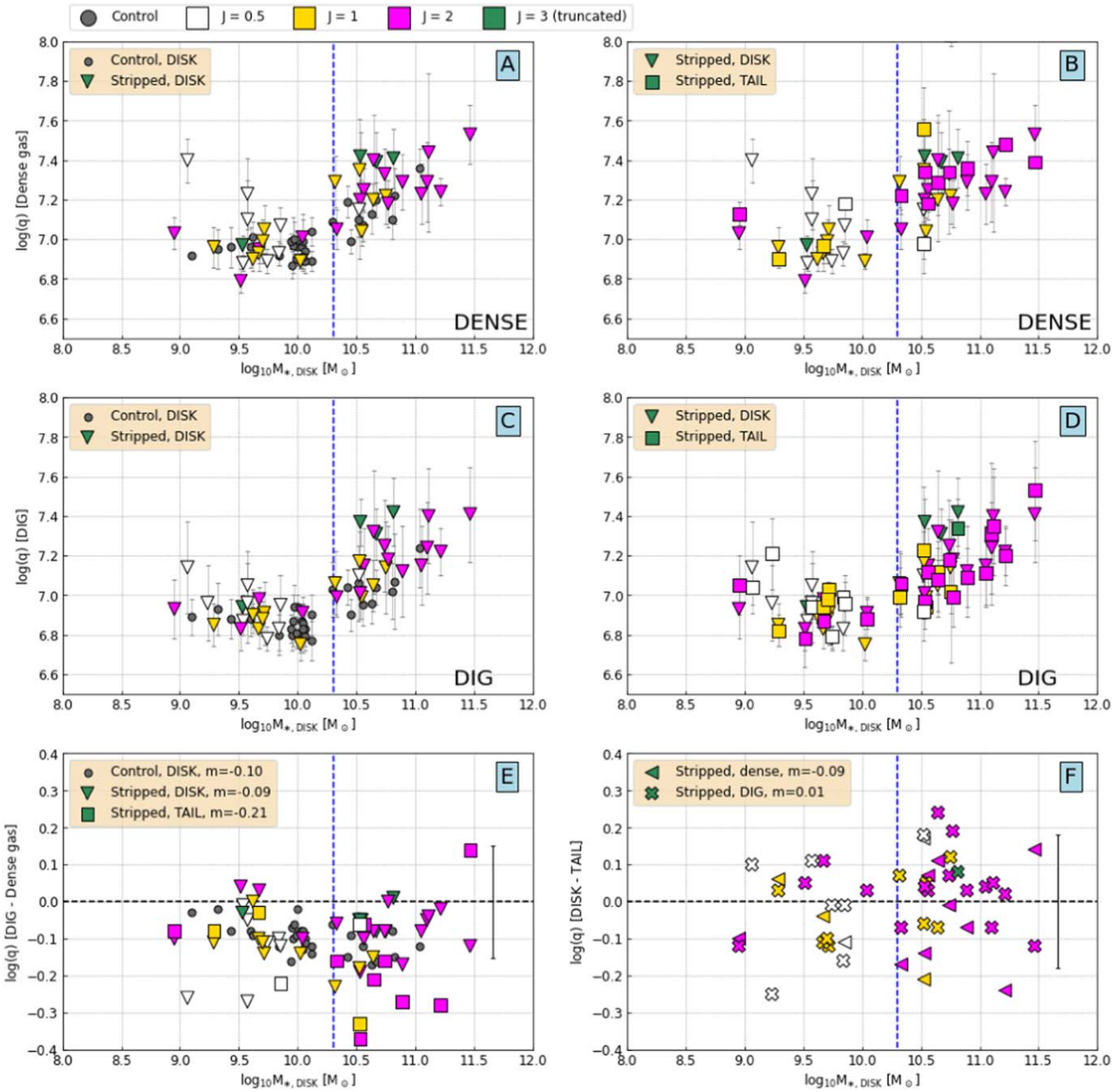

Figure 7. Panels A, B, C, and D show integrated (median of spaxels) values of log(q) as a function of galaxy stellar mass. Data points are color-coded by J stage (legend on the top). On the left panels (A and C) we compare disks of the control and stripped samples (with added tails in panel E), while on the right (panels B, D, and F) we compare the disks and tails of only stripped galaxies. We also separately present medians of the dense-gas-dominated regions (panels A and B) and medians from the DIG-dominated areas (panels C and D). In panel E, we show the difference between the DIG and dense-gas values, while in panel F we show the difference between the disks and tails of the stripped galaxies. The mean of the values shown in panels E and F is labeled in the legends for different parts of galaxies. The separation between low- and high-mass galaxies at $log_{10} M_* = 10.3$, used in previous sections, is indicated by the blue dashed line. The scatter of spaxel values for each galaxy is presented with error bars, while the mean of the data's error bars in panels E and F is presented with a single error bar on the right.

DIG in galaxy centers can exhibit bright $\Sigma H\alpha$ and low equivalent width, which could have biased the results of Zhang et al. (2017). Using data cubes from MaNGA and fiber spectroscopy from the Sloan Digital Sky Survey Data Release 7, Vale Asari et al. (2019) found that accounting for the DIG contribution leads to a change in metallicity of up to 0.1 dex, but can be negligible depending on the metallicity estimation method.

The major drawback of the methods of separating DIG and H II-dominated spaxels used by Poetrodjojo et al. (2019) and Zhang et al. (2017), is that they did not fully account for the effects of radial metallicity gradients on the [S II]/Hα ratio. On the other hand, a drawback of our method is that the low spatial resolution potentially can dilute the metallicity values of dense-gas spaxels, as discussed by Sánchez et al. (2014), Belfiore et al. (2017b), and Sánchez-Menguiano et al. (2018). This effect can lead to measuring similar metallicities between DIG and dense-gas spaxels in our sample.

4.2. Ionization Parameter

Our results at small spatial scales (≈ 1 kpc) lead us to conclude that DIG exhibits lower log(q) than dense gas (Figures 5 and 7).

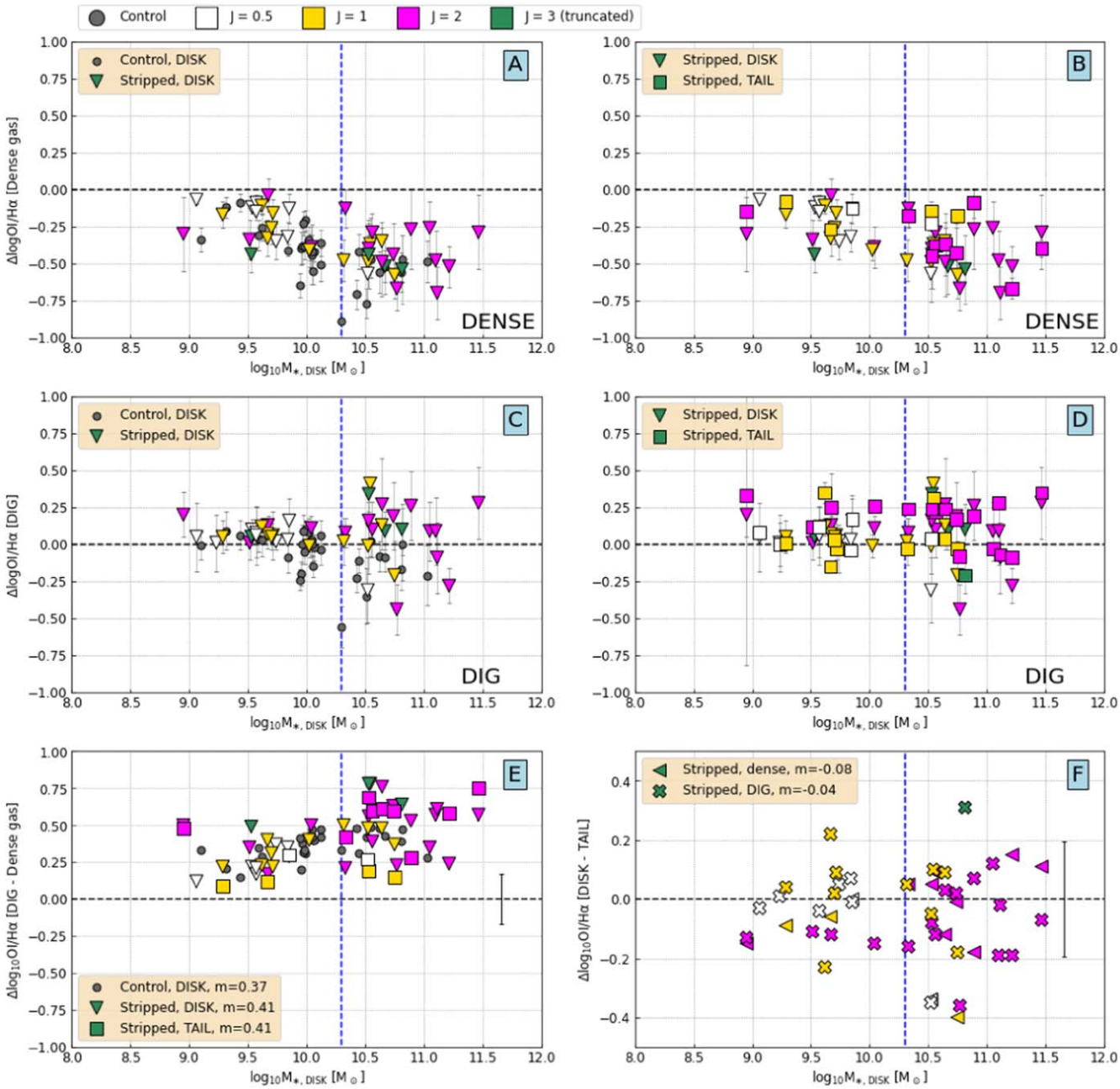

Figure 8. Same as in Figure 7, but for Δ log[O I]/Hα values, instead of log(q).

Similar conclusions have been drawn by Zhang et al. (2017) and Mingozzi et al. (2020) from their spatially resolved observations of log(q) in nearby galaxies. This is to be expected if we assume that the diffuse gas resides further from hot, young stars that are the source of a large number of ionizing photons. The only exceptions at those spatial scales are DIG-dominated spaxels in the edges of disks and in the tails of gas-stripped galaxies, which show an increase in log(q).

Another interesting aspect of our results is that high-mass galaxies show an anti-correlation between log(q) and galactocentric radius (Figure 5). We ascribe this increase to ionization due to a large number of HOLMES and evolved stars (Flores-Fajardo et al. 2011; Zhang et al. 2017) at decreasing galactocentric radius. Similarly, Dopita et al. (2014) observed higher log(q) values in the center of galaxies, and concluded that it is due to higher ΣSFR and changes in the geometry of the molecular and ionized gas. Simpson et al. (2007) observed an increase in excitation of gas toward the galactic center, probably due to shocks. On the other hand, Mingozzi et al. (2020) observed a correlation between log(q) and galactocentric radius, in high-mass galaxies. Similarly, Sánchez et al. (2012) and Sánchez et al. (2015) noted a weak correlation between those parameters.

There is an ongoing discussion about the relation between the ionizing parameter in galaxies and other integrated galactic properties. At galactic scales, we do not observe a strong effect of gas stripping on log(q), but we do note an increase in the log (q) range of the stripped galaxies compared to the control sample (Figure 6). However, this is the first study where a strong correlation between log(q) and the stellar mass for galaxies with $\log M_*/M_\odot > 10.3$ (Figure 7) is observed. We ascribe this trend to a higher fraction of HOLMES and evolved stars within high-mass galaxies compared to low-mass

galaxies. It is interesting that the tails also show an increase in $\log(q)$ with galaxy stellar mass, which may be a result of an interplay between gas and photon densities of the ISM. Integrated SFR and metallicities yield a positive correlation with $\log(q)$ probably due to their correlation with stellar mass. Similar to our observations, Dopita et al. (2014) observed a correlation between $\log(q)$ and SFR, while Poetrodjojo et al. (2018) did not.

4.3. Effects of Gas-stripping Process and $\Delta \log[O\,I]/H\alpha$

Our results indicate an increase in $\Delta \log[O\,I]/H\alpha$ toward the edges of galaxy disks (Figure 5) and a large fraction of DIG-dominated spaxels showing positive $\Delta \log[O\,I]/H\alpha$, designating them as LINER/LIER-like regions (Figure 3). In general, LINER/LIER-like features for DIG-dominated spaxels in the centers of non-stripped galaxies has been previously observed by Flores-Fajardo et al. (2011) and Zhang et al. (2017). Zhang et al. (2017) speculated that only ionization by evolved stars (older than 125 Myr) as a major ionization source for DIG can lead to LINER/LIER-like emission. The evolved stars and HOLMES may contribute to the increase in $\Delta \log[O\,I]/H\alpha$ within the disks of our sample (as seen in Figures 5 and 3).

The DIG areas in the tails of highly stripped galaxies (higher J-stage numbers) systematically exhibit the highest $\Delta \log[O\,I]/H\alpha$ values compared to the galactic disks (Figure 8). $\Delta \log[O\,I]/H\alpha$ correlates with distance from the SF regions in the disks and most of the tails (Figure 4). We also found that DIG in stripped tails extends to very large projected distances (Figure 4), and is spanning kpc and up to 10 kpc scales, which is larger than typical scale heights of galactic disks. The DIG at those large distances contributes to the increase in $\Delta \log[O\,I]/H\alpha$ and is showing LINER/LIER-like features. Those features are lacking in control galaxies. Previously, Poggianti et al. (2019b) observed that the tails of many gas-stripped galaxies in GASP exhibit LINER/LIER-like emission in BPT-[O I] diagrams, while the other diagnostic diagrams (based on NII or SII) suggest star formation or at least a composite origin for the ionization, which suggests that SF photons are partly the source of ionization.

In light of these results, we hypothesize that DIG in the edges and tails of stripped galaxies is ionized by more than one process (of which star formation may be one). Two competing candidates for that ionization are: (1) an older stellar population (older than 125 Myr and younger than 13 Gyr, as proposed by Flores-Fajardo et al. (2011) and Zhang et al. 2017) for ionization of DIG in galactic disks, or (2) mixing of hot–cold gas layers such as ICM and galactic ISM, as proposed by Slavin et al. (1993), Binette et al. (2009), and Poggianti et al. (2019a). The first option is less likely because the older stellar population would most likely form in SF knots of tails and would cover small distances from those SF regions. Although this candidate of ionizing DIG in tails should not be completely disregarded, we find the mixing of hot–cold gas layers and shocks more probable. This is also backed up by the findings of Poggianti et al. (2019a); Campitiello et al. (2021), and Müller et al. (2021), who found an excess in X-ray emission and the existence of magnetic fields in the tails of three of the jellyfish galaxies studied here, JO201, JW100, JO206. This X-ray excess may be produced by radiative cooling (Müller et al. 2021; Sparre et al. 2020) of the hot and highly magnetized ICM gas during the interplay with the galactic tail's ISM and accretion of the ICM onto the stripped ISM.

To conclude, we hypothesize that the gas-stripping process is creating galactic tails that are mixing with the ICM, thus ionizing the DIG at large distances from SF regions and systematically showing an increase in $\Delta \log[O\,I]/H\alpha$.

5. Conclusions

In this paper, we utilize the optical IFU (MUSE spectrograph) observations of 71 galaxies (30 control and 41 stripped) from the GASP project to analyze the gas properties of the dense and diffuse ionized gas. The investigated properties are gas-phase metallicity and ionization parameter $\log(q)$ for SF regions, and $\Delta \log[O\,I]/H\alpha$ values (the distance in the $OI/H\alpha$ value from the BPT-[O I] line that separates SF and LINER/LIER-like regions). We compare these properties between control sample and stripped galaxies, as well as between the disks and tails of the stripped galaxies. Our results indicate the following:

1. The DIG fraction does not strongly affect the gas-phase metallicity measurement at a given galactocentric radius, and thus does not affect the radial gradient metallicity across all of the galaxies.
2. The DIG-dominated areas mostly show lower $\log(q)$ compared to the dense-gas areas at small spatial scales. This is due to ionization of dense gas in the disks and most of the tails, coming from close and highly ionizing young stars.
3. $\log(q)$ spans a wider range in the stripped galaxies compared to the control sample, suggesting a larger spread in ionization parameter.
4. The integrated, galactic $\log(q)$ values correlate best with the total stellar mass, with more massive galaxies also showing an increase in $\log(q)$ in their galactic centers. We speculate that this increase is due to higher density of ionizing photons from older stellar populations that are dominating the central regions, and whose number is increasing at higher-galaxy masses.
5. The DIG systematically exhibits higher $\Delta \log[O\,I]/H\alpha$ compared to the dense gas and all galaxies show an increase in $\Delta \log[O\,I]/H\alpha$ and LINER/LIER-like features at their edges.
6. The gas-stripping process in galaxies creates tails of gas where mixing of the tail's ISM and ICM both ionize DIG and cause an increase in $\Delta \log[O\,I]/H\alpha$ values. The areas of highest $\Delta \log[O\,I]/H\alpha$ reside in the tails of highly stripped galaxies (highest J-stage number), in areas at large distances (up to 10 kpc) from the SF regions. These distances indicate that neither the SF regions alone nor the older stellar population alone nor a combination of both can explain the ionization of DIG.

These findings suggest that the gas-stripping process does not affect metallicities, nor does it have a strong effect on the ionization parameter, but has strong effects of gas stripping on $\Delta \log[O\,I]/H\alpha$.

Our results shed additional light on the process of ram pressure that affects the ionized gas and star formation in galaxies. In the future, we aim to further investigate the dust and stellar ultraviolet emission of DIG-dominated regions versus dense regions, both in normal disks and disks and tails of stripped galaxies.

The authors kindly thank Giovanni Fasano, who estimated positions and radii of Hα clumps for the GASP project. Based on observations collected at the European Organization for Astronomical Research in the Southern Hemisphere under ESO program 196.B-0578. This project has received funding from the European Research Council (ERC) under the European Union's Horizon 2020 research and innovation program (grant agreement No. 833824). We acknowledge financial contribution from the contract ASI-INAF n.2017-14-H.0, from the grant PRIN MIUR 2017 n.20173ML3WW_001 (PI: Cimatti), and from the INAF mainstream funding program (PI: Vulcani). J.F. acknowledges financial support from the UNAM-DGAPA-PAPIIT IN111620 grant, Mexico. This work made use of Astropy, a community-developed core Python package for Astronomy (Astropy Collaboration et al. 2013), and MPFIT (Markwardt 2009).

Facilities: MUSE, ESO.

Software: Astropy (Astropy Collaboration et al. 2013), KUBEVIZ (Fossati et al. 2016), MPFIT (Markwardt 2009), PYQZ (v0.8.2; Dopita et al. 2013; Vogt et al. 2015), SINOPSIS (Fritz et al. 2017).

Appendix
Δ log[O I]/Hα and log(*q*) of Integrated Data

As in Figures 7 and 8, in this section we compare integrated log (*q*) and Δ log[O I]/Hα as a function of a disk's SFR (Figure 9),

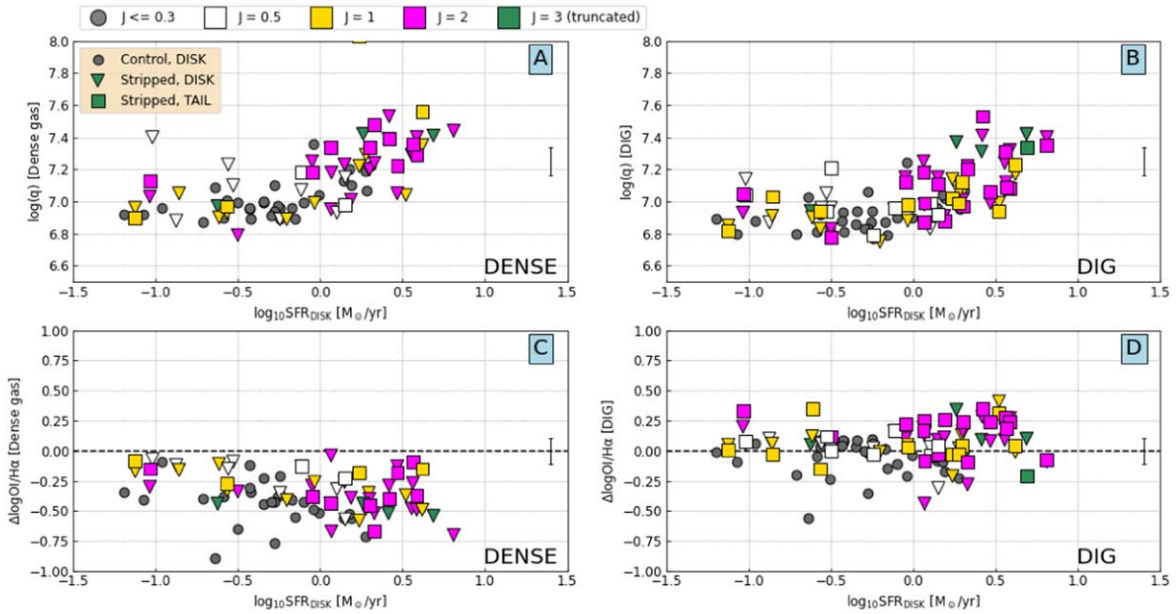

Figure 9. Median of log(*q*) (panels A and B) and Δ log[O I]/Hα (panels C and D) values for galaxies as a function of SFR. The galaxies are color-coded by J stage (labeled on the top), only showing galaxies with large enough numbers of spaxels in their disks and tails. We present disks of the control and stripped samples and tails of the stripped galaxies. We separated the median of the dense-gas-dominated regions (panels A and C) from medians from the DIG-dominated areas (panels B and D). With the error bar on the right, we show median of all error bars for individual galaxies.

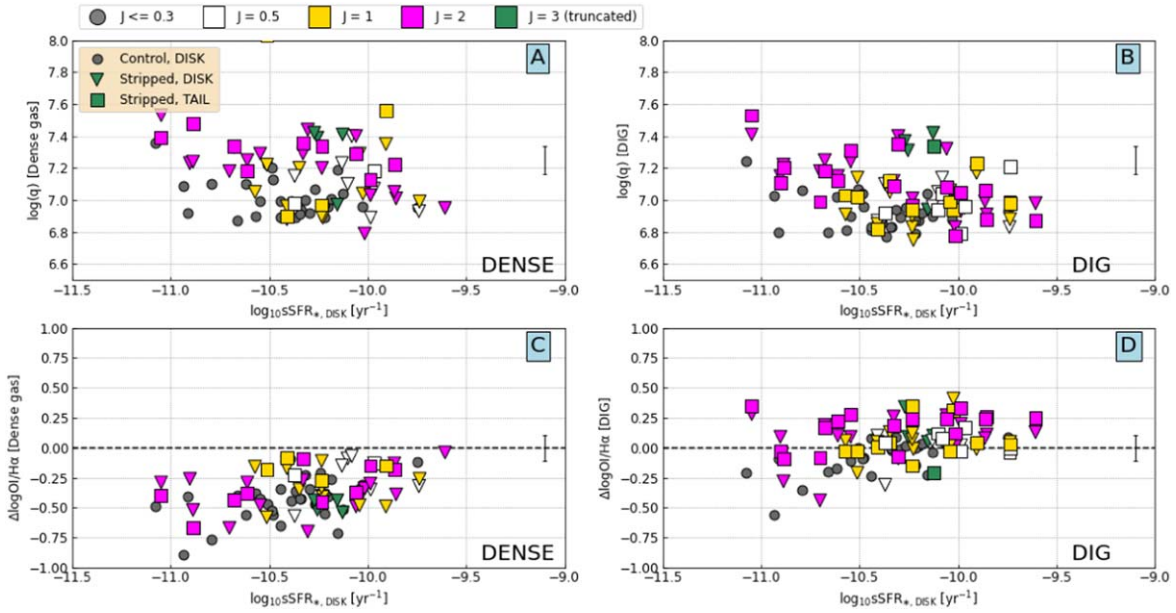

Figure 10. Same as Figure 9, but with specific SFR (sSFR) on the *x*-axis.

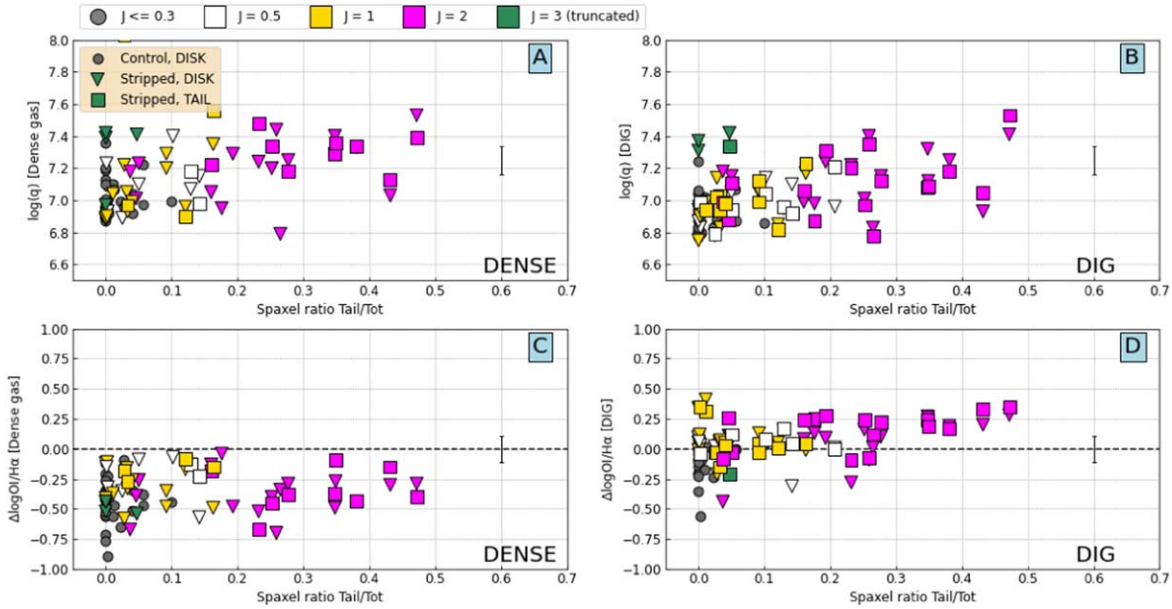

Figure 11. Same as Figure 9, but with ratio of numbers of spaxels from tail and disk on the *x*-axis.

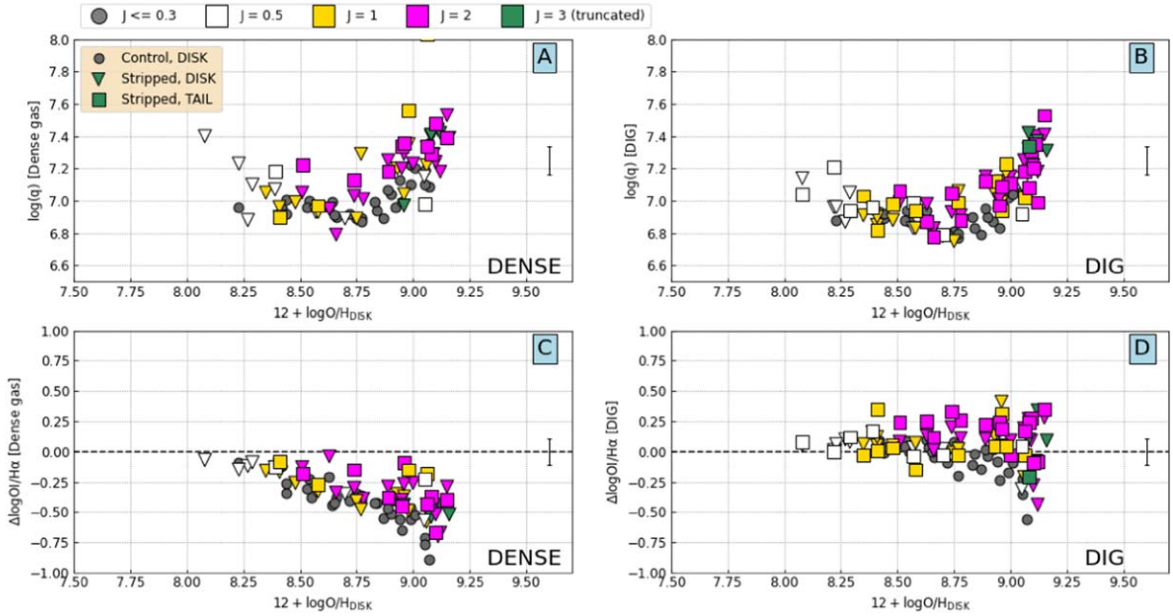

Figure 12. Same as Figure 9, but with gas-phase metallicity on the *x*-axis.

sSFR (Figure 10), ratio of number of spaxels from tails and disks (Figure 11), and gas-phase metallicity (Figure 12). We separate the dense-gas- and DIG-dominated data in these figures and mark the data according to J stage (by color) or by which type or part of galaxies they represent (type of marks).

We hypothesize that the SFR and gas-phase metallicity correlate to the mass of the stellar disk (Franchetto et al. 2020), thus the behavior seen in the figures can be explained by a variation in the mass instead of a correlation with $\Delta \log[\mathrm{O\,I}]/\mathrm{H}\alpha$ and $\log(q)$. Similar correlations between integrated $\log(q)$ and SFR and metallicity were also observed by Tremonti et al. (2004) and Dopita et al. (2014). Furthermore, the metallicity values may be affected by $\log(q)$ measurements, so trends seen in Figure 12 may yield a wrong interpretation. For the sSFR and the spaxel number ratio of tails versus disks, we do not see a clear correlation in $\Delta \log[\mathrm{O\,I}]/\mathrm{H}\alpha$ and $\log(q)$.

ORCID iDs

Neven Tomičić https://orcid.org/0000-0002-8238-9210
Benedetta Vulcani https://orcid.org/0000-0003-0980-1499
Bianca M. Poggianti https://orcid.org/0000-0001-8751-8360
Marco Gullieuszik https://orcid.org/0000-0002-7296-9780
Anna Wolter https://orcid.org/0000-0001-5840-9835
Mario Radovich https://orcid.org/0000-0002-3585-866X
Alessia Moretti https://orcid.org/0000-0002-1688-482X
Andrea Franchetto https://orcid.org/0000-0001-9575-331X
Jacopo Fritz https://orcid.org/0000-0002-7042-1965

References

Astropy Collaboration, Robitaille, T. P., Tollerud, E. J., et al. 2013, A&A, 558, A33
Bacon, R., Bauer, S., Boehm, P., et al. 2006, Proc. SPIE, 6269, 183
Baldwin, J. A., Phillips, M. M., & Terlevich, R. 1981, PASP, 93, 5
Barnes, J. E., Wood, K., Hill, A. S., & Haffner, L. M. 2014, MNRAS, 440, 3027
Belfiore, F., Maiolino, R., Maraston, C., et al. 2016, MNRAS, 461, 3111
Belfiore, F., Maiolino, R., Maraston, C., et al. 2017a, MNRAS, 466, 2570
Belfiore, F., Maiolino, R., Tremonti, C., et al. 2017b, MNRAS, 469, 151
Binette, L., Drissen, L., Ubeda, L., et al. 2009, A&A, 500, 817
Blanc, G. A., Heiderman, A., Gebhardt, K., Evans, N. J. I., & Adams, J. 2009, ApJ, 704, 842
Bocchio, M., Bianchi, S., Hunt, L. K., & Schneider, R. 2016, A&A, 586, A8
Bundy, K., Bershady, M. A., Law, D. R., et al. 2015, ApJ, 798, 7
Calvi, R., Poggianti, B. M., & Vulcani, B. 2011, MNRAS, 416, 727
Campitiello, M. G., Ignesti, A., Gitti, M., et al. 2021, ApJ, 911, 144
Cardelli, J. A., Clayton, G. C., & Mathis, J. S. 1989, ApJ, 345, 245
Chabrier, G. 2003, PASP, 115, 763
Cid Fernandes, R., Stasińska, G., Mateus, A., & Vale Asari, N. 2011, MNRAS, 413, 1687
Collins, J. A., & Rand, R. J. 2001, ApJ, 551, 57
Consolandi, G., Gavazzi, G., Fossati, M., et al. 2017, A&A, 606, A83
Cowie, L. L., & Songaila, A. 1977, Natur, 266, 501
Della Bruna, L., Adamo, A., Bik, A., et al. 2020, A&A, 635, A134
Dopita, M. A., Rich, J., Vogt, F. P. A., et al. 2014, Ap&SS, 350, 741
Dopita, M. A., Sutherland, R. S., Nicholls, D. C., Kewley, L. J., & Vogt, F. P. A. 2013, ApJS, 208, 10
Fasano, G., Marmo, C., Varela, J., et al. 2006, A&A, 445, 805
Flores-Fajardo, N., Morisset, C., Stasińska, G., & Binette, L. 2011, MNRAS, 415, 2182
Fossati, M., Fumagalli, M., Boselli, A., et al. 2016, MNRAS, 455, 2028
Franchetto, A., Vulcani, B., Poggianti, B. M., et al. 2020, ApJ, 895, 106
Fritz, J., Moretti, A., Gullieuszik, M., et al. 2017, ApJ, 848, 132
Fumagalli, M., Fossati, M., Hau, G. K. T., et al. 2014, MNRAS, 445, 4335
Gullieuszik, M., Poggianti, B., Fasano, G., et al. 2015, A&A, 581, A41
Gullieuszik, M., Poggianti, B. M., McGee, S. L., et al. 2020, ApJ, 899, 13
Gunn, J. E., Gott, J., & Richard, I. 1972, ApJ, 176, 1
Haffner, L. M., Dettmar, R. J., Beckman, J. E., et al. 2009, RvMP, 81, 969
Heckman, T. M., & Balick, B. 1980, A&A, 83, 100
Herpich, F., Stasińska, G., Mateus, A., Vale Asari, N., & Cid Fernandes, R. 2018, MNRAS, 481, 1774
Hoopes, C. G., & Walterbos, R. A. M. 2003, ApJ, 586, 902
Hummer, D. G., & Storey, P. J. 1987, MNRAS, 224, 801
Kaplan, K. F., Jogee, S., Kewley, L., et al. 2016, MNRAS, 462, 1642
Kewley, L. J., Dopita, M. A., Sutherland, R. S., Heisler, C. A., & Trevena, J. 2001, ApJ, 556, 121
Kewley, L. J., Groves, B., Kauffmann, G., & Heckman, T. 2006, MNRAS, 372, 961
Kewley, L. J., Nicholls, D. C., & Sutherland, R. S. 2019, ARA&A, 57, 511
Koopmann, R. A., & Kenney, J. D. P. 2004, ApJ, 613, 851
Kreckel, K., Blanc, G. A., Schinnerer, E., et al. 2016, ApJ, 827, 103
Kumari, N., Maiolino, R., Belfiore, F., & Curti, M. 2019, MNRAS, 485, 367
Lacerda, E. A. D., Cid Fernandes, R., Couto, G. S., et al. 2018, MNRAS, 474, 3727
Levy, R. C., Bolatto, A. D., Sánchez, S. F., et al. 2019, ApJ, 882, 84
Madsen, G. J., Reynolds, R. J., & Haffner, L. M. 2006, ApJ, 652, 401
Maier, C., Lilly, S. J., Carollo, C. M., et al. 2006, ApJ, 639, 858
Markwardt, C. B. 2009, in ASP Conf. Ser., 411, Astronomical Data Analysis Software and Systems XVIII, ed. D. A. Bohlender, D. Durand, & P. Dowler (San Francisco, CA: ASP), 251
Martin, C. L. 1997, ApJ, 491, 561
Mingozzi, M., Belfiore, F., Cresci, G., et al. 2020, A&A, 636, A42
Minter, A., & Balser, D. S. 1998, LNP, 506, 543
Minter, A. H., & Spangler, S. R. 1997, ApJ, 485, 182
Müller, A., Poggianti, B. M., Pfrommer, C., et al. 2021, NatAs, 5, 159
Nagao, T., Maiolino, R., & Marconi, A. 2006, A&A, 459, 85
Oey, M. S., Meurer, G. R., Yelda, S., et al. 2007, ApJ, 661, 801
Osterbrock, D. E., & Martel, A. 1992, PASP, 104, 76
Otte, B., Gallagher, J. S. I., & Reynolds, R. J. 2002, ApJ, 572, 823
Poetrodjojo, H., D'Agostino, J. J., Groves, B., et al. 2019, MNRAS, 487, 79
Poetrodjojo, H., Groves, B., Kewley, L. J., et al. 2018, MNRAS, 479, 5235
Poggianti, B. M., Gullieuszik, M., Tonnesen, S., et al. 2019b, MNRAS, 482, 4466
Poggianti, B. M., Ignesti, A., Gitti, M., et al. 2019a, ApJ, 887, 155
Poggianti, B. M., Moretti, A., Gullieuszik, M., et al. 2017, ApJ, 844, 48
Raymond, J. C. 1992, ApJ, 384, 502
Relaño, M., Kennicutt, R. C. J., Eldridge, J. J., Lee, J. C., & Verley, S. 2012, MNRAS, 423, 2933
Reynolds, R. J. 1984, ApJ, 282, 191
Reynolds, R. J., & Cox, D. P. 1992, ApJL, 400, L33
Reynolds, R. J., Sterling, N. C., Haffner, L. M., & Tufte, S. L. 2001, ApJL, 548, L221
Sánchez, S. F. 2020, ARA&A, 58, 99
Sánchez, S. F., Galbany, L., Pérez, E., et al. 2015, A&A, 573, A105
Sánchez, S. F., Rosales-Ortega, F. F., Iglesias-Páramo, J., et al. 2014, A&A, 563, A49
Sánchez, S. F., Rosales-Ortega, F. F., Marino, R. A., et al. 2012, A&A, 546, A2
Sánchez-Menguiano, L., Sánchez, S. F., Pérez, I., et al. 2018, A&A, 609, A119
Sanders, R. L., Shapley, A. E., Zhang, K., & Yan, R. 2017, ApJ, 850, 136
Scaife, A. M. M. 2013, AdAst, 2013, 390287
Schlafly, E. F., & Finkbeiner, D. P. 2011, ApJ, 737, 103
Schlegel, D. J., Finkbeiner, D. P., & Davis, M. 1998, ApJ, 500, 525
Searle, L. 1971, ApJ, 168, 327
Simpson, J. P., Colgan, S. W. J., Cotera, A. S., et al. 2007, ApJ, 670, 1115
Singh, R., van de Ven, G., Jahnke, K., et al. 2013, A&A, 558, A43
Slavin, J. D., Shull, J. M., & Begelman, M. C. 1993, ApJ, 407, 83
Sparre, M., Pfrommer, C., & Ehlert, K. 2020, MNRAS, 499, 4261
Tomičić, N., Kreckel, K., Groves, B., et al. 2017, ApJ, 844, 155
Tomičić, N., Vulcani, B., Poggianti, B. M., et al. 2021, ApJ, 907, 22
Toomre, A., & Toomre, J. 1972, ApJ, 178, 623
Tremonti, C. A., Heckman, T. M., Kauffmann, G., et al. 2004, ApJ, 613, 898
Vale Asari, N., Couto, G. S., Cid Fernandes, R., et al. 2019, MNRAS, 489, 4721
Vila-Costas, M. B., & Edmunds, M. G. 1992, MNRAS, 259, 121
Vogt, F. P. A., Dopita, M. A., Borthakur, S., et al. 2015, MNRAS, 450, 2593
Vulcani, B., Moretti, A., Poggianti, B. M., et al. 2017, ApJ, 850, 163
Vulcani, B., Poggianti, B. M., Gullieuszik, M., et al. 2018a, ApJL, 866, L25
Vulcani, B., Poggianti, B. M., Jaffé, Y. L., et al. 2018c, MNRAS, 480, 3152
Vulcani, B., Poggianti, B. M., Moretti, A., et al. 2018b, ApJ, 852, 94
Vulcani, B., Poggianti, B. M., Moretti, A., et al. 2019a, MNRAS, 487, 2278
Vulcani, B., Poggianti, B. M., Moretti, A., et al. 2019b, MNRAS, 488, 1597
Vulcani, B., Poggianti, B. M., Moretti, A., et al. 2021, ApJ, 914, 27
Vulcani, B., Poggianti, B. M., Tonnesen, S., et al. 2020, ApJ, 899, 98
Weingartner, J. C., & Draine, B. T. 2001, ApJS, 134, 263
Werle, A., Cid Fernandes, R., Vale Asari, N., et al. 2020, MNRAS, 497, 3251
Yeh, S. C. C., & Matzner, C. D. 2012, ApJ, 757, 108
Zhang, K., Yan, R., Bundy, K., et al. 2017, MNRAS, 466, 3217